

Extracellular matrix composition and interstitial pH modulate NHE1-mediated melanoma cell motility

ANNE-KRISTIN VAHLE^{1,5}, BRITTA DOMIKOWSKY², CHRISTIAN SCHWÖPPE³, HERMANN KRÄHLING¹, SABINE MALLY¹, MICHAEL SCHÄFERS⁴, SVEN HERMANN⁴, VICTOR SHAHIN¹, JÖRG HAIER², ALBRECHT SCHWAB¹ and CHRISTIAN STOCK¹

¹Institute of Physiology II, ²Department of General and Visceral Surgery, ³Department of Hematology and Oncology, ⁴European Institute of Molecular Imaging, University of Münster, D-48149 Münster, Germany

Received July 26, 2013; Accepted August 30, 2013

DOI: 10.3892/ijo.2013.2158

Abstract. The activity of the Na⁺/H⁺ exchanger NHE1 is required for human melanoma cell adhesion and migration. The goal of the present study was to suppress mouse melanoma (B16V) cell invasion *in vivo* by inhibiting NHE1. Intravital observations in mobilized left liver lobes of laparotomized male Sprague-Dawley rats disclosed that five minutes after intra-arterial administration of the B16V cell suspension, cells adhered to the endothelia of liver sinusoidal capillaries and started to migrate into the surrounding liver tissue. In the presence of the NHE1-specific inhibitor cariporide, migration/invasion was reduced by about 50% while adhesion was not lowered. Time-lapse video microscopy and adhesion/invasion assays revealed that *in vitro*, blockade of NHE1 by cariporide i) significantly decreased the migratory speed of the cells and ii) completely inhibited the invasive behavior of both an artificial, basement membrane-like and a dermis-like matrix. Cells were more motile on the basement membrane and more invasive on the dermis-like matrix. Small-animal PET (positron-emission tomography) analyses of B16V metastasis in female C57BL/6 mice showed that, although NHE1 inhibition hardly affected the percentage of animals developing metastases or relapses, metastases seem to get directed to the lungs in cariporide-treated animals while animals feeding on the standard diet show metastases spread all over the body. We conclude that i) B16V cells prefer to invade a dermis-like rather than a basement membrane-like matrix; ii) the extracellular matrix (ECM) composition

strongly impacts on NHE1-dependent *in vitro* cell motility and invasion; and iii) the lungs are metastasis-prone and impair the efficiency of cariporide due to their ECM composition and the pulmonary interstitial (extravascular) pH.

Introduction

Metastasis is a multistep process based on a series of events called the metastatic cascade. Neoplastic cells break away from the primary tumor, invade the neighboring tissue and intravasate into existing or newly formed lymph or blood vessels, circulate within the bloodstream and adhere to vascular walls somewhere else in the body. At these distant sites, the adherent cells extravasate through the endothelium of specific target organs, invade the surrounding tissue and proliferate to form a secondary or metastatic tumor. This chain of events requires the cells to have migration ability.

Tumor cell migration is a complex process that includes the degradation of the extracellular matrix (ECM) by the activity of tumor cell-secreted matrix metalloproteinases (MMPs) as well as a coordinated formation and release of focal adhesion contacts to the extracellular matrix mediated by receptor molecules such as integrin dimers (1). Focal adhesion contacts are small, stable, yet transient interactions between the cell and the ECM (2,3). In addition to a number of cytosolic proteins attached to the actin filament network such as the proteins of the ezrin/moesin/radixin family (4), the ubiquitously expressed Na⁺/H⁺ exchanger isoform 1, NHE1, is also part of these focal adhesion contacts where it may interact with integrins either directly or indirectly via the translocated protons (5-8).

The activity of NHE1 is important for various tumor cell behavior (9,10). The insufficient tumor vascularization characteristic of solid tumors and cancer-related anaemia lead to an inadequate O₂ supply so that the metabolism of the tumor cells is mostly glycolytic. But also in the presence of oxygen tumor cells can perform glycolysis [Warburg effect (11)]. Hence, tumor cells are often confronted with an increased acid load (12). The protons initially accumulating in the cytosol are extruded into the extracellular space by NHE1 which then causes an extracellular acidification of the surrounding tissue.

Activation of NHE1 is required for cell polarity and migration in fibroblasts (13), epithelial MDCK cells (14) and

Correspondence to: Dr Christian Stock, Institute of Physiology II, University of Münster, Robert-Koch-Str. 27b, D-48149 Münster, Germany
E-mail: cmstock@uni-muenster.de

Present address: ⁵Department of Otorhinolaryngology, University Hospital of Essen, University of Duisburg-Essen, Hufelandstrasse 55, D-45147 Essen, Germany

Key words: cariporide, cell adhesion, cell migration, metastasis, NHE1

human melanoma cells (15). It enhances the invasiveness of human breast carcinoma cells (16,17) and affects migration, morphology and adhesion of human melanoma cells (15). These observations imply that NHE1 is involved in metastasis and tumor malignancy.

One phenomenon in metastasis is the so-called organotropism (18), i.e. the preference of cancer cells to metastasize to characteristic target organs. Thus, in addition to regional metastasis along the draining lymph nodes close to the primary tumor, distant melanoma metastases are primarily found in the lungs including the area between the lungs, in liver, skin and brain (19). The more than a century-old 'seed and soil' theory postulates that while the cancer cells ('the seed') can disseminate into various organs through circulation, they can thrive only in permissive tissues ('the soil') that match the intrinsic properties of the tumor cell (20). However, the reasons for this organo- or tissue tropism appear to be diverse and for the most part the underlying mechanisms are hardly understood. The direct, physical tumor-stroma interaction strongly affects the development of metastases in different tissues and organs. Composition, structure and stiffness of the extracellular matrix can modulate cell motility by exerting haptic stimuli (21). An ECM that is optimally resistant to cell-generated tractional forces is capable of promoting maximal migration speeds. At the same time invasion requires an ECM that is digestible for the matrix metalloproteinase set that the cells are equipped with. Both, adhesion to the ECM as well as its digestion require an optimum pH at the cell surface (22). In addition to the overall proton concentration present in the stroma, NHE1 activity represents a tunable proton source (15,23,24).

Taking advantage of an *in vivo* approach we show that inhibiting NHE1 activity does, indeed, reduce invasion of B16V melanoma cells into liver tissue by 50% while directing metastases to the lungs. To explain this striking observation and to learn more about the compatibility of a tumor cell with its surrounding ECM the present study compares the NHE1-dependent adhesion, migration, invasion and ECM digestion of the murine B16V melanoma cell line on two different matrices whose composition resemble either that of the basement membrane or that of the ECM of the dermis.

Materials and methods

Cells and cell culture. Cells of the mouse melanoma cell line B16V (25) were grown in bicarbonate buffered RPMI-1640 (Sigma, Taufkirchen, Germany) supplemented with 10% (v/v) FBS at 37°C in a humidified atmosphere of 5% CO₂/95% air.

Experimental solutions. *In vitro* cell migration, adhesion and invasion were observed in serum free RPMI-1640 medium. Desired pH values were adjusted by adding appropriate amounts of NaHCO₃.

pH measurements were performed using HEPES-buffered Ringer solutions containing (mmol l⁻¹): 122.5 NaCl, 5.4 KCl, 0.8 MgCl₂, 1.2 CaCl₂, 1.0 NaH₂PO₄·2H₂O, 5.0 glucose, 10 HEPES. A pH of 7.0 was adjusted by adding 1 M NaOH.

Where applicable the NHE1 inhibitor cariporide (HOE642, final concentration: 10 μmol l⁻¹) was added to either the serum free media or to the HEPES-buffered Ringer solution.

Detection of NHE1 by western blot analysis. We followed a protocol by Fafournoux *et al.* (26). Confluent cells were washed twice with an ice-cold, hypotonic solution containing (mmol l⁻¹): 3 KCl, 5 EDTA, 10 Tris-HCl (pH 7.4). Cells were lysed at 4°C for 10 min in lysis buffer consisting of the hypotonic solution containing 1.0 mmol l⁻¹ Pefabloc SC Plus (Roche Molecular Biochemicals, Mannheim, Germany) and 0.2% (v/v) of a protease inhibitor cocktail (Sigma, P8340). Lysates were scraped off 10-cm culture dishes (BD Falcon, Franklin Lakes, NJ, USA), homogenized and spun down at 20,800 x g. The pellets were resuspended in the hypotonic solution and mixed with reducing sample buffer (4:1, v/v) containing 500 mmol l⁻¹ Tris, 100 mmol l⁻¹ dithiothreitol, 8.5% SDS, 27.5% sucrose and 0.03% bromophenol blue indicator. SDS-PAGE was performed using acrylamide gels (7.5%) and a Minigel System (Bio-Rad Laboratories, Hercules, CA, USA). Equal amounts of protein were loaded. Electroblothing was performed at 0.8 mA cm⁻² for 50 min. The nitrocellulose membranes (Schleicher & Schuell, Dassel, Germany) carrying the blotted proteins were bathed in 5% (w/v) milk in 0.1% (v/v) Tween in PBS for 1 h at room temperature and then washed with 0.1% Tween in PBS. Overnight incubation with the primary antibody to the NHE1 (BD Biosciences Pharmingen, 1:500) at 4°C was followed by a 1-h incubation with a horseradish peroxidase-conjugated goat anti-mouse IgG (1:10,000) at room temperature. Blots were developed using an ECL immunoblotting detection reagent kit (Amersham, Arlington Heights, IL, USA).

Measuring intracellular pH (pH_i). pH_i was measured using video imaging techniques and the fluorescent pH indicator BCECF (Molecular Probes, Eugene, OR, USA) as previously described (15). Cells were treated as for migration experiments, resuspended in HEPES-buffered Ringer solution (pH 7.0), plated onto collagen coated coverslips and allowed to adapt for 3 h. Cells were then incubated with BCECF-AM (final concentration: 2 μmol l⁻¹) for 5 min. The coverslips were placed on the stage of an inverted microscope (Axiovert 200; Carl Zeiss Inc., Göttingen, Germany) and continuously superfused with prewarmed (37°C) HEPES-buffered Ringer solutions (for composition see Experimental solutions in Materials and methods). The excitation wavelengths alternated between 440 and 488 nm, respectively, while the emitted fluorescence intensities were monitored at 520 nm using a Photometrics camera (CoolSnapfx, Visitron Systems, Puchheim, Germany). The different wavelengths were generated by a high speed polychromator system (Visichrome, Visitron Systems). Polychromator and data acquisition were controlled by Metafluor software (Visitron Systems). Fluorescence intensities were measured in 35-sec intervals and corrected for background fluorescence. At the end of each experiment, the pH measurements were calibrated by superfusing the B16 cells successively with modified Ringer solutions of pH 7.5, 7.0 and 6.5 containing (mmol l⁻¹): 125 KCl, 1 MgCl₂, 1 CaCl₂, 20 HEPES and 10 μmol l⁻¹ nigericin (Sigma-Aldrich).

Invasion into rat liver parenchyma. Male Sprague-Dawley rats (200 to 250 g, Charles River) were cared for in accordance with standards of the German Council on Animal Care, under an approved protocol of the local Animal Welfare Committee. Rats were anesthetized using inhalation of isoflurane (Curamed, Karlsruhe, Germany) and N₂O and prepared as previously

described (27,28). Vital signs and oxygenation status were kept stable throughout the experiments. For intravital observation of adhesive interactions between circulating tumor cells and the hepatic microcirculation, single-cell suspensions of 1×10^6 CalceinAM fluorescent-labeled B16V cells with or without $600 \mu\text{mol l}^{-1}$ cariporide were injected intra-arterially over 60 sec. Mobilized left liver lobes of the laparotomized rats were placed on a specific holder in order to investigate the lower lobe surface while avoiding disturbances of hepatic blood flow. Throughout the experiments the liver was continuously irrigated with isotonic saline solution. A x20 objective was located above a cover slip covering the organ surfaces. A semi-quantitative analysis of tumor cell adhesions and extravasation was performed over a 30 min observation period. Using a standardized procedure, all fields were analyzed in each of the 5-min intervals. Cells were divided into i) merely adherent and ii) extravasating cells and their average numbers in 30 microscopic fields were counted. Fluorescence images were recorded employing a video-enhancer-zoom lens system, a low-light charge-coupled device video camera allowing real-time imaging via a separate monitor and a timer containing S-VHS video system for further analysis.

Reconstituting extracellular matrices. Two different matrices were prepared, i) a basement membrane-like matrix and ii) a dermis-like matrix. In detail, the basement membrane-like matrix consisted of HEPES-buffered, serum free RPMI-1640 containing (mg ml^{-1}): 0.32 collagen type IV (BD Biosciences, Heidelberg, Germany), 0.0025 laminin (Sigma-Aldrich) and 0.025 fibronectin (Roche). The dermis-like matrix, also mixed in serum-free RPMI-1640, contained (mg ml^{-1}): 2.53 collagen type I (Biochrom AG, Berlin, Germany), 0.083 collagen type IV and 0.01875 laminin. The pH of both collagen mixtures was adjusted to 7.4 by adding 1 M NaOH.

For migration experiments the bottoms of 25-ml culture flasks (12.5 cm^2 , BD Falcon) were covered with $200 \mu\text{l}$ of the collagen mixture each, and the matrices were allowed to polymerize overnight at 37°C in a humidified atmosphere.

For adhesion assays each well of a 24-multiwell plate (BD Falcon) was coated with $80 \mu\text{l}$ of the collagen mixture, and for invasion assays filter membranes with a pore size of $8.0 \mu\text{m}$ (ThinCert™, Greiner Bio-One) were coated with $60 \mu\text{l}$ of the collagen mixture. The matrices were allowed to polymerize overnight at 37°C in a humidified atmosphere.

Scanning the matrix surfaces. Atomic force microscopy was employed to scan the surfaces of the two matrices. To this end the matrices polymerized on glass coverslips overnight at 37°C in a humidified atmosphere. They were then air-dried. The coverslips coated with the air-dried matrices were mounted on little metal plates using double-faced adhesive tape. In order to scan the surfaces of the matrices we used a Multimode AFM (NanoScope V controller, Veeco, Santa Barbara, CA, USA) equipped with a stereo microscope. Gold coated, V-shaped silicon nitride cantilevers (MSCT, Veeco) with a spring constant of 0.03 N m^{-1} and pyramidal tips with an estimated tip radius of 10 nm were used. The images were recorded with 512 scan lines per area, at constant force (height mode) in contact mode in air with a scan rate of 3-5 Hz. Images were processed using the Nanoscope 7.0 software (Veeco). High-resolution imaging of the matrices demanded fine-tuning of the scanning

process. This comprised mainly the minimizing of the scanning force between tip and sample to values below 3 nN.

Cell adhesion and invasion. For adhesion, B16V cells grown to confluency were resuspended in serum free culture medium with or without $10 \mu\text{mol l}^{-1}$ cariporide and then seeded on matrix-coated plates (10×10^4 cells per well) inserted in a 24-multiwell plate (BD Falcon). After 3 h the media including the non-adhesive cells were washed off with cold PBS buffer, the remaining cells were fixed with 3.5% paraformaldehyde in PBS and counted.

For invasion, 90,000 cells were seeded on matrix-coated filter-membranes with pore sizes of $8.0 \mu\text{m}$ (ThinCert, Greiner Bio-One) at the three pH values, pH 6.8, 7.0 and 7.5. After a 48-h incubation cells were fixed and stained with crystal violet. The matrix and the remaining cells on the upper side of the filter were removed carefully and excess crystal violet was washed away with distilled water. The invasive cells that remained on the lower side of the filter were counted. To exclude that possible differences in the cell numbers are based on pH-dependent proliferation rates a proliferation assay was performed. Cells (90,000) were seeded in small cell culture dishes (area 1.9 cm^2). After a 48-h incubation including changing the media after 24 h, the cells were trypsinized and the cell density was determined. From the numbers obtained for the cell density the factor by which the number of cells had increased due to proliferation was calculated. The number of cells found on the lower side of the matrix-coated filter membrane was divided by this 'proliferation factor' in order to receive the correct number of invasive cells.

Analyzing cell migration. The matrix-coated culture flasks were put into heated chambers on stages of inverted microscopes (Axiovert25, Carl Zeiss Inc.). Cell migration was recorded in 10-min intervals for 5 h at 37°C using video cameras (Models XC-ST70CE and XC-77CE, Hamamatsu/Sony, Japan) and PC-vision frame grabber boards (Hamamatsu, Herrsching, Germany). Acquisition of images was controlled by HiPic and WASABI software (Hamamatsu). The cell contours were labeled applying AMIRA software (TGS, San Diego, CA, USA) and served as the basis for further analysis. Parameters such as structural index (SI), migratory velocity ($\mu\text{m min}^{-1}$) and translocation (μm) were analyzed using self-made JAVA programs and the NIH ImageJ software (<http://rsb.info.nih.gov/ij/>). Migration was determined as the movement of the cell center per time unit, the velocity was estimated from the 10-min time intervals applying a three point difference quotient and the cell area was measured as the number of pixels. The structural index (SI) represents the cell shape and was calculated as follows: $\text{SI} = (4 \pi A)/p^2$, where A is the area covered by the cell and p is the perimeter of A. Values close to 1 correspond to a spherical cell shape whereas values close to 0 correspond to a spindle or a dendritic cell shape.

Detecting extracellular matrix digestion using in situ zymography. The quenched fluorophore Bodipy (Invitrogen, Darmstadt, Germany) was used for analysis of ECM proteolysis *in vitro*. In the intact molecule, the fluorescence is quenched by about 95% so that fluorescence occurs only when the protein is proteolyzed.

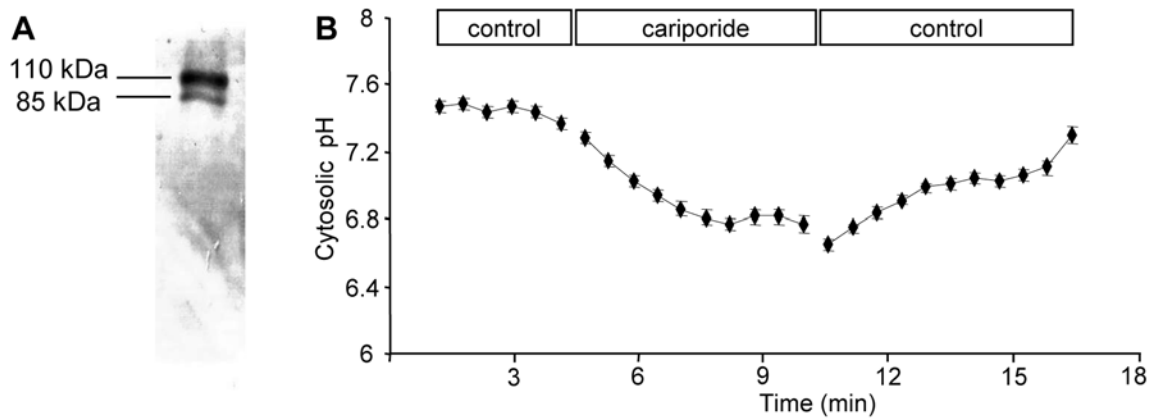


Figure 1. NHE1 is present and reversibly inhibitable in the B16V mouse melanoma cell line. (A) NHE1 as detected by western blot analysis. The two characteristic bands of i) the completely glycosylated (N- and O-glycosides) NHE1 as predominantly present in the plasma membrane and ii) the N-glycosylated NHE1 as present in the endoplasmic reticulum were found at 110 and 85 kDa, respectively. (B) Cytosolic pH was measured prior to, during and after NHE1 inhibition with 10 $\mu\text{mol l}^{-1}$ cariporide. The cariporide-induced intracellular acidification from pH 7.4 to pH 6.8 and the reversibility of this effect upon removal of the inhibitor (pHi 7.2) clearly indicate that NHE1 is involved in the pH homeostasis of B16V cells (mean \pm SD, n=150 cells from 12 independent trials, pHi 7.2).

The *in situ* zymography was performed as described previously by Busco *et al.* (29). The two matrices were prepared as described above. Prior to the polymerization step, BSA-Bodipy-fluorescein conjugate (Invitrogen) was added cautiously to the matrix components (final concentration 30 $\mu\text{g ml}^{-1}$) and mixed by gentle shaking. A total of 200 μl of the mix was distributed uniformly on a coverslip (\varnothing 30 mm) and allowed to polymerize overnight at 37°C in a humidified atmosphere. Per coverslip approximately 30,000 cells were seeded and allowed to adhere and spread on the matrix at 37°C in a humidified atmosphere of 5% CO₂/95% air. Three or six hours after seeding cells were fixed with paraformaldehyde (3.5% in PBS) and focal digestion was visualized by fluorescence microscopy. To this end, the coverslips were placed on the stage of an inverted microscope (Axiovert 200, Carl Zeiss Inc.). The excitation wavelength of 488 nm was set by a high speed polychromator (Visichrome, Visitron Systems, Puchheim, Germany). Emission intensity was monitored at 510 nm using a Photometrics camera (CoolSnapfx). Polychromator and data acquisition were controlled by Metafluor software (Visitron Systems). The overall fluorescence intensity underneath the entire cell was corrected for background fluorescence by subtracting background intensities.

Metastasis in mice. C57BL/6 mice (Harlan, Horst, The Netherlands) were cared for in accordance with standards of the German Council on Animal Care, under an approved protocol of the local Animal Welfare Committee. A total of 80 μl of a B16V cell suspension containing 12.8x10⁶ cells ml⁻¹ in PBS were intradermally transplanted into the right flanks of 10-week-old female C57BL/6 mice. Mice fed standard or a cariporide containing (0.6% v/v) diet (Altromin, Lage, Germany), starting immediately after transplantation. After 3 weeks, the primary tumor was removed and metastasis was monitored over a period of 7 weeks employing a small-animal PET followed by autopsies of the eventually sacrificed animals. 2-Deoxy-2-[¹⁸F]fluoro-D-glucose (¹⁸F-FDG)-PET was used to evaluate the glucose utilization of tumors. Uptake of radioactivity was visualized using the high resolution quadHIDAC

small animal PET scanner [Oxford Positron Systems; spatial resolution 0.7 mm FWHM (30)]. Mice were anesthetized with isoflurane inhalation (2% in oxygen) and temperature was maintained by using a heating pad during the experimental procedure. Radiotracer (10 MBq) was injected intravenously and image acquisition at 60-75 min p.i. was performed.

Statistics. All experiments were repeated three to thirteen times. Data are presented as the mean values \pm SD or SEM as indicated. The data were tested for significance employing Student's unpaired or paired t-test or analysis of variance (ANOVA) where applicable. The level of significance was set at p<0.05 (*p<0.05; **p<0.01; ***p<0.001).

Results

NHE1 expression and activity in B16V cells. The present study intended to transfer the knowledge on the function of NHE1 in single human melanoma (MV3) cell migration to a murine melanoma cell line and to translate it into an *in vivo* system. We chose B16V cells as they fulfil two requirements: they express NHE1 as shown by western blot analysis (Fig. 1A) and inhibiting their NHE1 activity with the specific inhibitor cariporide induces the expected reversible intracellular acidification (Fig. 1B).

B16V *in vivo* invasion requires NHE1 activity. As the main aim of the present study was to prove that inhibition of NHE1 affects B16V cell adhesion and invasion not only *in vitro* but also *in vivo*, fluorescently labeled B16V cells and cariporide or its solvent alone were injected into the carotid arteries of rats. As previously demonstrated this route of injection ensured highest reproducibility and avoided a relevant artificial first pass effect within the lungs. The number of cells adhering to the vessel walls of liver sinusoids and that of cells extravasating into the surrounding liver parenchyma were counted. During the first 5 min after injection of the cell suspension about 25 cells (total number, obtained from 30 visual fields per rat) had already adhered to the vessel wall (Fig. 2A and C). After

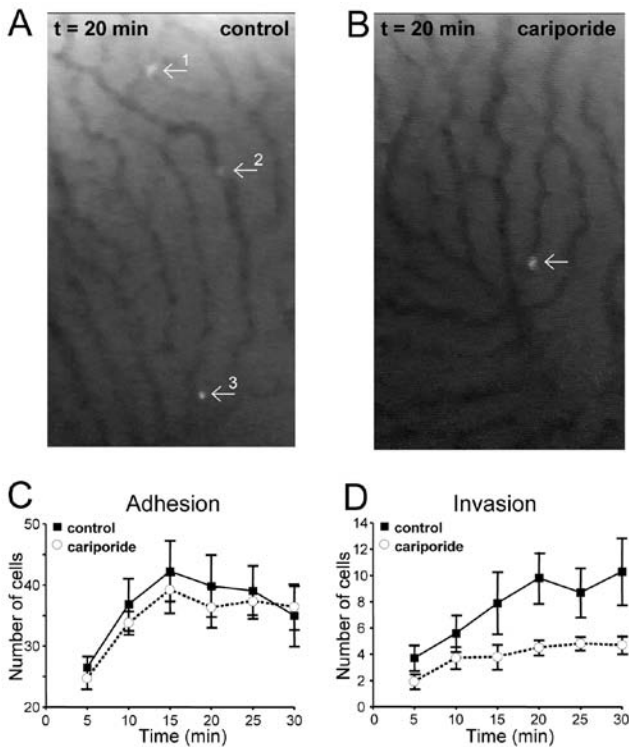


Figure 2. *In vivo* adhesion and migration of B16V melanoma cells in a rat liver preparation does not depend on NHE1 activity (A and C) whereas *in vivo* migration in(to) the parenchyma clearly does (B and D). (A) Micrograph of rat liver tissue. Sinusoids can be distinguished from liver parenchyma by their darker color. Cells 1 and 3 invaded the liver parenchyma while cell 2 remains adherent to the sinusoid wall. (B) Typically, in the presence of cariporide adherent cells do not extravasate but remain inside the sinusoid as shown here for a single cell. (C and D) Summary of $n=7$ experiments (rats). Inhibiting NHE1 with $10 \mu\text{mol l}^{-1}$ cariporide has no effect on adhesion (C), whereas it reduces the number of cells invading the liver tissue by 50% (D). Data are presented as mean values \pm SD. Blood pH is assumed to range between pH 7.2 and 7.4, areas shown in (A) and (B) are 0.2 mm^2 .

15 min cell adhesion had reached its maximum at about 40 adherent cells. There was no significant difference in the cell adhesiveness in the presence or absence of the NHE1-inhibitor cariporide (39 ± 3 vs. 42 ± 5 , respectively). In contrast, invasion starting within the initial 5 min after injection was clearly dependent on NHE1 activity (Fig. 2B and D). In the presence of cariporide the number of cells found to be migrating inside the liver parenchyma was reduced by 50%. This held true for the entire time span beginning at $t=5$ min until the end of the observation period at $t=30$ min.

Surface structure of reconstituted matrices. Since human melanoma cell adhesion to a reconstituted collagen type I matrix depends on NHE1 activity (31) we theorized that the lack of the cariporide effect on B16V adhesion to the sinusoidal wall could be caused by the composition of the local, perisinusoidal matrix, known to be rich in fibronectin (32). To identify how the ECM composition affects the behavior of B16V cells, two different ECMs, a basement membrane-like and a dermis-like matrix, were prepared. Their relief was scanned utilizing the AFM technique. The basement membrane-like matrix formed a dense gel with hardly visible, very small pores compared to the dimension of a cell (Fig. 3A) whereas the dermis-like

matrix formed a fibrillar meshwork with large pores (Fig. 3B). This observation is perfectly consistent with electron micrographs published by Poincloux *et al* (33) who compared the matrix architecture of Matrigel commonly used to imitate the basement membrane with that of acid-solubilized collagen I often used as a model for the interstitial matrix.

The basement membrane-like matrix facilitates adhesion and migration. Fig. 4 shows that B16V cells were significantly more adhesive ($p < 0.05$) on the basement membrane-like as compared to the dermis-like matrix (Fig. 4A and B). On both matrices, particularly on the basement membrane-like matrix, inhibition of NHE1 activity by cariporide led to a decrease in adhesiveness [95.8 ± 8.7 vs. 29.1 ± 2.3 cells per visual field on the basement membrane-like matrix ($p < 0.001$), 34.0 ± 7.6 vs. 21.5 ± 5.2 cells per visual field on the dermis-like matrix ($p < 0.05$)]. We chose two parameters to describe cell motility: i) the migratory speed (Fig. 4C); and ii) the translocation that represents the distance covered during the course of a 5-h experiment (Fig. 4D). B16V cells travelled almost twice as fast when seeded on the basement membrane-like matrix (0.4 ± 0.03 vs. $0.25 \pm 0.03 \mu\text{m min}^{-1}$, $p < 0.05$). On both matrices the migratory speed was clearly reduced by the specific NHE1 inhibitor cariporide (basement: -20% ; $0.32 \pm 0.03 \mu\text{m min}^{-1}$, $p = 0.04$; dermis: -38% ; $0.16 \pm 0.02 \mu\text{m min}^{-1}$, $p = 0.04$). In contrast, the translocation remained nearly unaffected on the basement membrane but was significantly lowered on the dermis-like matrix (from 27.3 ± 7.0 to $11.4 \pm 2.2 \mu\text{m}$, $p < 0.05$).

The dermis-like matrix facilitates invasion. Next, we investigated whether the matrix-dependent differences in the migratory behavior of B16V cells are reflected also in their invasive behavior (Fig. 4E and F). The cells preferred to invade the dermis-like matrix. Invasion into the dermis-like matrix was drastically reduced upon NHE1 inhibition by cariporide. Normally, invasion is accompanied by digestion of the extracellular matrix (34). According to this and to our observation that B16V cells prefer to invade the dermis-like matrix, the cells digested the dermis-like matrix much more efficiently than the basement membrane-like matrix (Fig. 5A and B). Also the digestion process is significantly facilitated by the activity of NHE1.

B16V cell adhesion, morphology, migration and invasion depend on extracellular pH_e . At extracellular pH (pH_e) values of 6.8 and 7.0, NHE1 inhibition by cariporide led to a significant ($p < 10^{-3}$) decrease in *in vitro* cell adhesion (Fig. 6A). This cariporide effect was most distinct at acidic pH_e values (pH_e 6.8) and not present at pH_e 7.5. Adhesion also depended on pH_e *per se* irrespective of NHE1 activity. It decreased as pH_e increased no matter whether NHE1 was fully active (pH_e 6.8: 40.9 ± 12.2 ; pH_e 7.0: 34.0 ± 7.6 ; pH_e 7.5: 14.5 ± 6.4 cells per well) or inhibited (pH_e 6.8: 24.5 ± 7.3 ; pH_e 7.0: 21.5 ± 5.2 ; pH_e 7.5: 11.4 ± 4.5 cells per well). At the same time the morphology altered from spindle-shaped to spherical (Fig. 6B and C). Accordingly, the structural index (Fig. 6B) increased by approximately 0.15 units in control and in cariporide-treated cells when pH_e was shifted from pH 7.0 to 7.5. However, in general, cariporide-treated cells were significantly more spherical than the cells under control conditions.

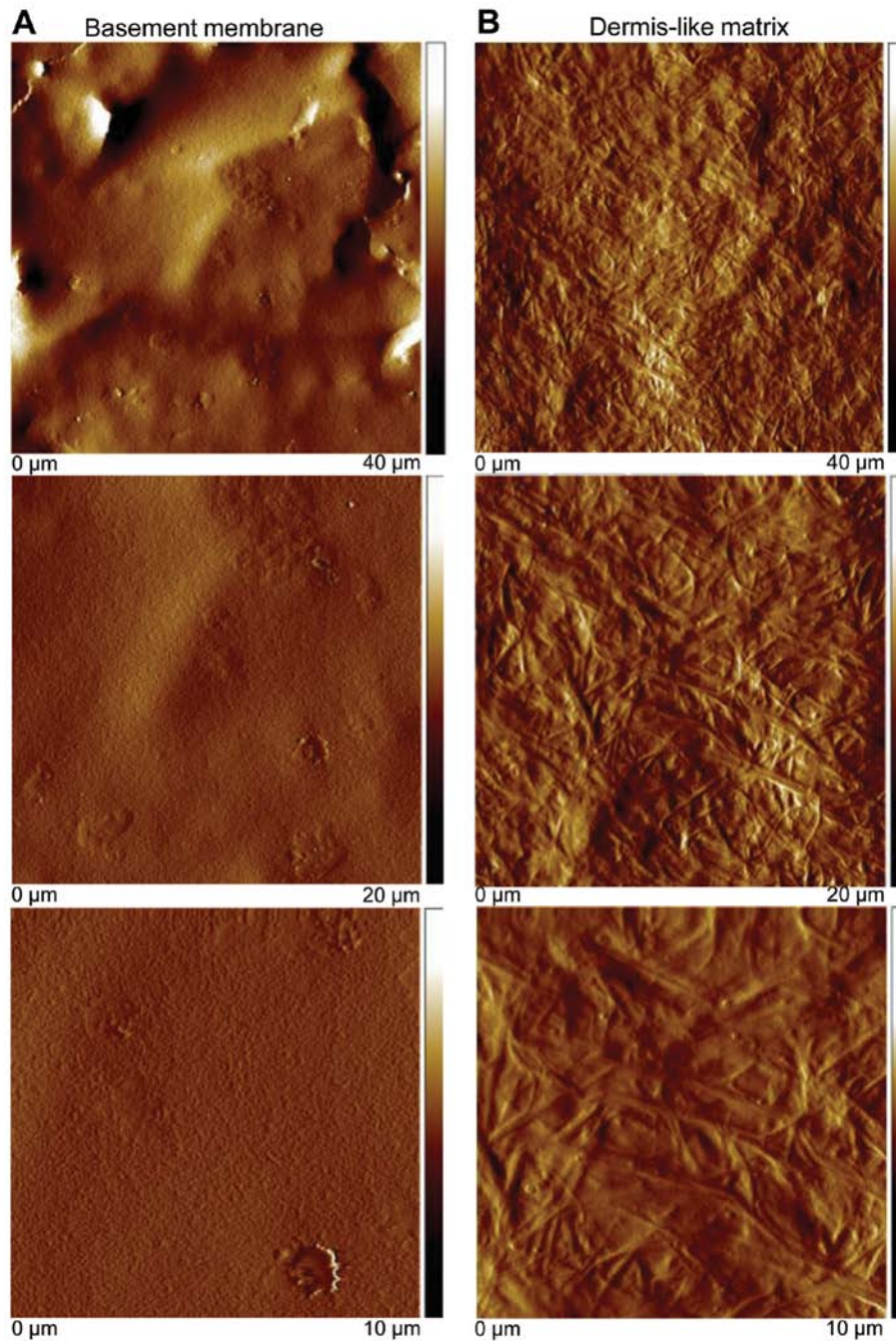


Figure 3. Atomic force microscopy images of reconstituted matrices. (A) The basement membrane-like matrix composed of collagen IV (92.1%), fibronectin (7.2%) and laminin (0.7%) forms a dense, rather even matrix with small pores and point-shaped elevations. (B) The dermis-like or interstitial-like matrix consisting of collagen I (96.1%), collagen IV (3.2%) and laminin (0.7%) forms a typical, fibrillar and spaced meshwork. Images represent squares of 40 x 40, 20 x 20 or 10 x 10 μm^2 . The color-coded bars illustrate the height.

Migration of B16V cells depends also on pH_e (Fig. 6D and E). Under standard conditions at pH_e 7.0 maximum migratory speed was $0.25 \pm 0.03 \mu\text{m min}^{-1}$ (Fig. 6D) and the translocation amounted to $27.3 \pm 7.0 \mu\text{m}$ (Fig. 6E). From there, speed and translocation decreased when pH_e was increased to pH 7.5 (speed: $0.15 \pm 0.02 \mu\text{m min}^{-1}$, translocation: $10.9 \pm 2.0 \mu\text{m}$) or decreased to pH 6.8 (speed: $0.23 \pm 0.03 \mu\text{m min}^{-1}$, translocation: $18.4 \pm 3.6 \mu\text{m}$). NHE1 inhibition led to a significant reduction in migratory speed at all of the different pH_e values. A lower pH_e seems to be able to compensate for the lack of NHE1 activity: in cariporide treated cells the migratory activity, i.e. speed and

distance, increased continuously as pH_e decreased from pH 7.5 (speed: $0.08 \pm 0.01 \text{ min}^{-1}$, translocation: $9.7 \pm 1.6 \mu\text{m}$) over pH 7.0 (speed: $0.16 \pm 0.02 \mu\text{m min}^{-1}$, translocation: $11.4 \pm 2.2 \mu\text{m}$) to pH 6.8 (speed: $0.17 \pm 0.03 \mu\text{m min}^{-1}$, translocation: $14.0 \pm 3.2 \mu\text{m}$).

Invasion was completely absent at all tested pH_e values when NHE1 was inhibited by cariporide (Fig. 6F). In contrast, under control conditions invasion reached its maximum at pH_e 7.0 (28.5 ± 10.0 cells per filter). It dropped significantly when pH_e was increased to pH 7.5 (8.6 ± 2.8 cells per filter) and was also diminished when pH_e was decreased to pH 6.8 (16.3 ± 6.7 cells per filter).

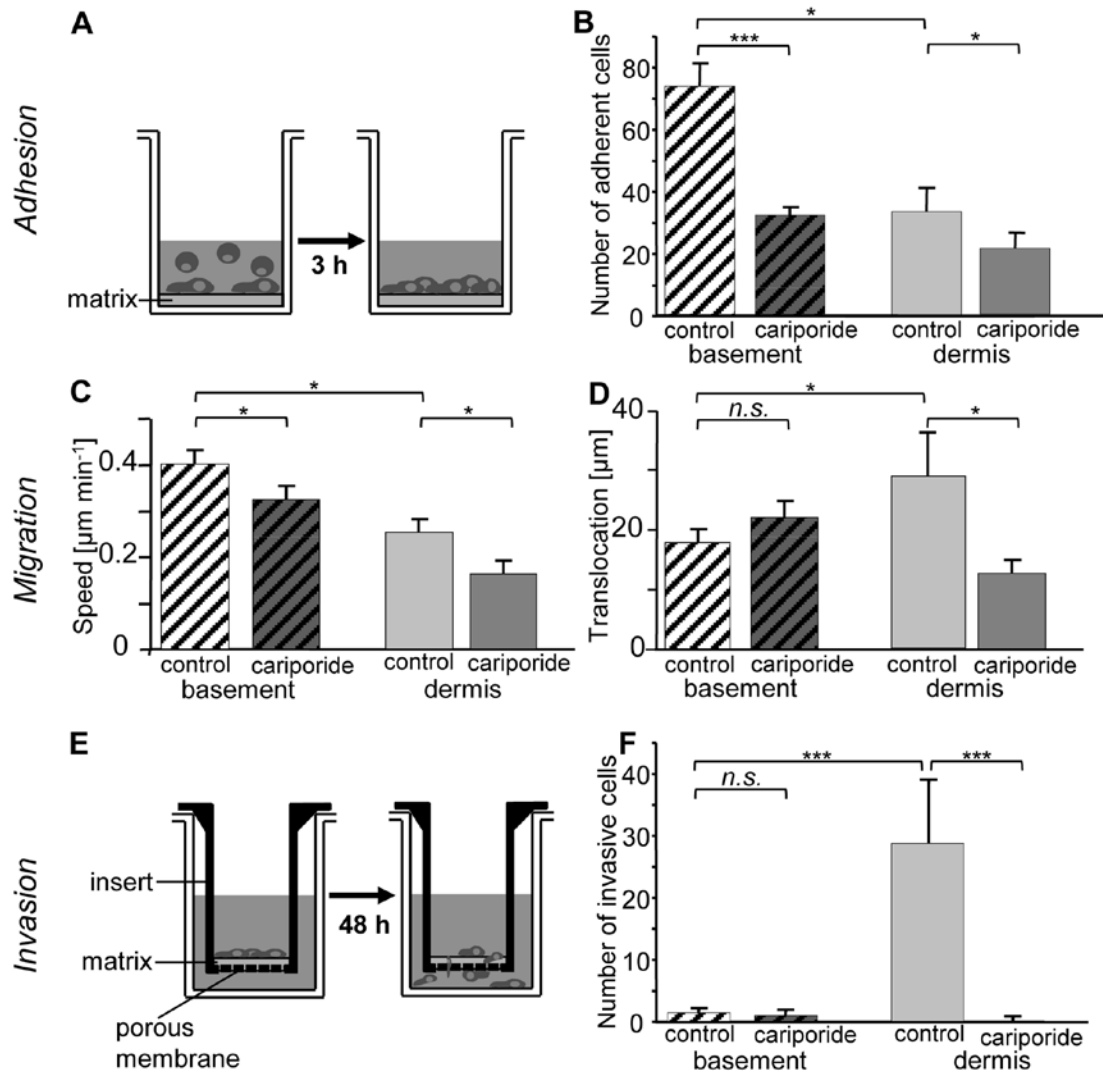


Figure 4. Adhesion, migration and invasion of murine melanoma (B16V) cells depend on ECM composition and NHE1 activity. (A) Three hours after seeding loose cells were washed away and remaining cells were counted ($n=13$ independent experiments). (B) At an extracellular pH of 7.0 adhesion of B16V cells is only half as strong on the dermis-like compared to the basement-like matrix, and in both cases, it is significantly reduced upon NHE1 inhibition by cariporide. (C and D) Migration given as speed (C) and as translocation (the net distance covered) within 5 h (D) depends on the composition of the extracellular matrix ($n =$ at least 30 cells from 8 experiments in each case). While the migratory speed is generally higher on the basement membrane-like matrix, the distance covered is more sensitive to NHE1 inhibition in cells seeded on the dermis-like matrix. (E) Cells were seeded on the two different matrices in absence and presence of the NHE1 inhibitor cariporide. Cells were allowed to invade the matrix and cross the porous bottom of the insert for a period of 48 h. Cells at the lower surface of the porous membrane were counted ($n=8$ experiments). (F) B16V cells invade the dermis-like but hardly the basement membrane-like matrix. Invasion is completely inhibited in the presence of cariporide. All data are presented as mean values \pm SEM.

NHE1-inhibition affects melanoma metastasis. In addition to the intravital imaging of B16V cell invasion into rat liver parenchyma (Fig. 2), we launched another *in vivo* approach investigating NHE1-dependent metastasis in female C57BL/6 mice. Three weeks after intradermal injection of the B16V cell suspension into the right flank, the primary tumor was removed and metastasis was monitored over a period of 7 weeks employing a small-animal PET and followed by autopsies of the finally sacrificed animals (Fig. 7). The percentage of animals developing metastases or local relapses hardly differed between the two groups. In 4 out of the 8 (50%) control animals and in 5 out of the 8 (62.5%) cariporide-treated animals metastases and/or local relapses occurred after removal of the primary tumor. However, it is particularly noticeable that counting all visible metastases per animal revealed that in cariporide-treated

animals metastases occurred mainly in the lungs (in 3 out of the 4 control vs. 5 out of the 5 cariporide-treated animals), but neither in the dermis nor in lymph nodes. Metastases in the ovaries were rather rare compared to untreated animals. Thus, in cariporide-treated cells metastases seem to get directed to the lungs while control animals show metastases spread all over the body.

Discussion

Key results of the present study are that NHE1 inhibition in B16V cells i) significantly reduces invasion of rat liver parenchyma; ii) decreases adhesion, migration and invasion depending on the composition of the employed reconstituted matrices; and iii) directs the metastatic spread to the lungs.

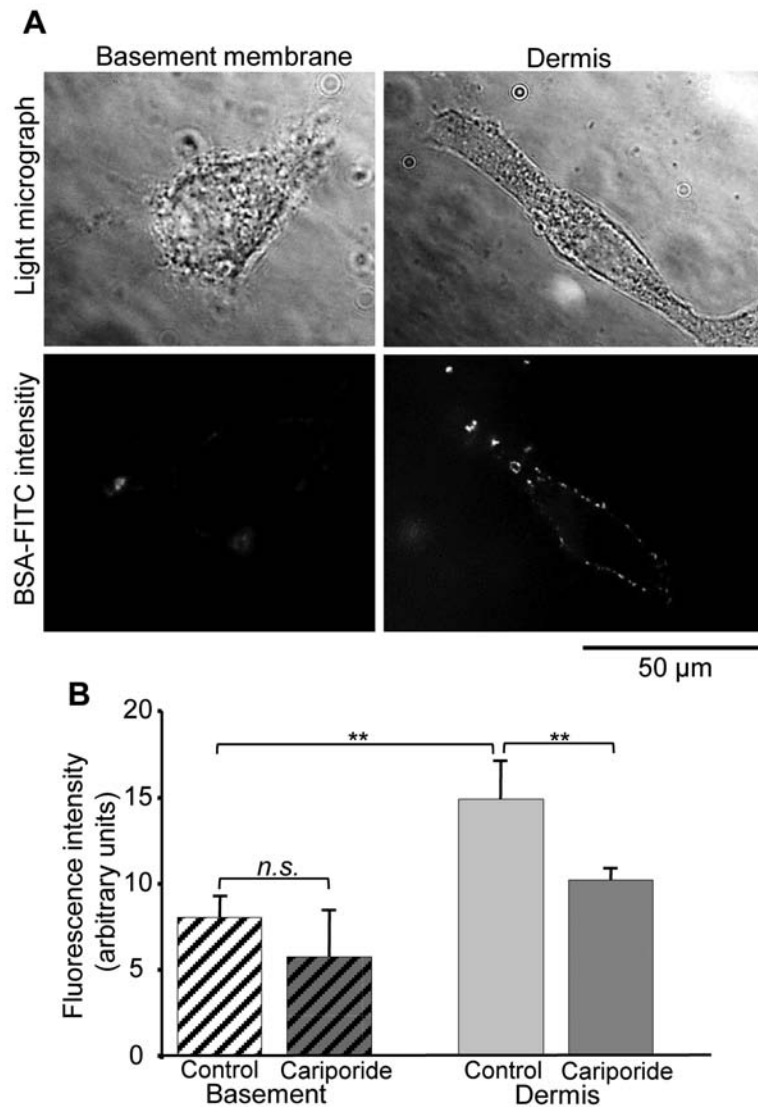


Figure 5. Enzymatic ECM digestion depends on the ECM composition and NHE1 activity. The matrices contained BSA-Bodipy-fluorescein conjugate ($30 \mu\text{g ml}^{-1}$). (A) ECM digestion results in dequenching of the fluorophore as protein fragments containing isolated fluorophores are released. (B) The fluorescence intensity per cell area was determined and taken as a measure for digestion ($n = \text{at least } 10 \text{ cells per condition, mean } \pm \text{ SEM}$).

NHE1 inhibition efficiently reduces invasion of liver parenchyma. B16V cell adhesion to the walls of rat liver sinusoids was observed to remain unaffected by cariporide whereas invasion of the liver parenchyma was decreased by $\sim 50\%$ (Fig. 2). Collagen types I, III, IV and V are the most frequently found in the ECM of the rat liver (35). While collagen types I, III and V are confined mainly to the portal tract and the central vein wall, type IV collagen, laminin and fibronectin are components of a low-density, basement membrane-like material lining the sinusoidal walls (36,37). The low density of this basement membrane-like structure could help the tumor cells to adhere to the sinusoidal wall and to find access to the parenchyma. The ECM of the liver parenchyma also contains heparan sulfate-proteoglycans (38,39). The heparan sulfate-proteoglycans are digested by the B16 cells' MMPs, thereby allowing efficient B16 invasion of the rat liver parenchyma (40). While NHE1 inhibition by cariporide hardly affects adhesion to the sinusoidal wall, it significantly reduces invasion suggesting that under these conditions the protons

extruded by NHE1 function as a digestive catalyzing MMP action rather than as a glue that strengthens focal adhesions (22). This interpretation finds additional support by our *in vitro* studies showing that the physiological pH close to ~ 7.4 in the sinusoidal blood possibly renders cariporide ineffective in disturbing adhesion (Fig. 6A) whereas invasion is significantly reduced even at pH 7.4 (Fig. 6F).

The ECM composition arranges motility and invasion. In order to analyze B16V migration and invasion more precisely, two types of reconstituted matrices resembling either the ECM of the dermis or the basement membrane were generated (Fig. 3). B16V cell behavior was totally different on these two matrices. Cells were more adhesive and migrated more quickly on the basement membrane while strongly invading the dermis-like matrix. These findings support the observations by Luikart *et al* (41) who found that a B16 clone derived from B16F1 remained more spherical when seeded on collagen type I whereas it tended to spread on collagen type IV. In the

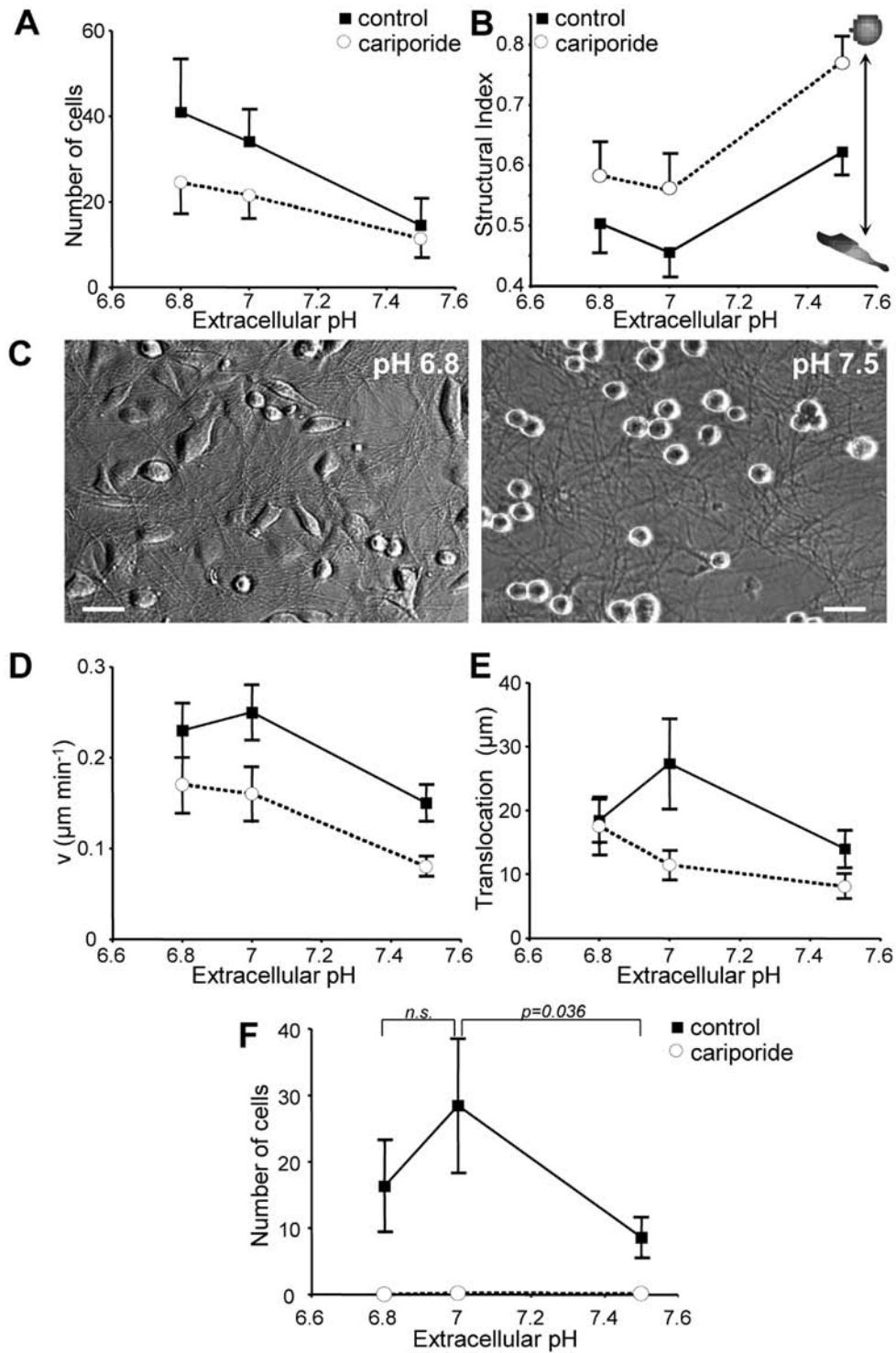


Figure 6. In B16V cells seeded on a dermis-like matrix, adhesion, morphology, migration and invasion depend on extracellular pH (pH_e). (A) Cell adhesion decreases as the extracellular pH increases. Inhibiting NHE1 with cariporide lowers adhesiveness at more acidic extracellular pH rather than at physiologically relevant pH_e values (mean \pm SEM, $n=13$ experiments). (B) The structural index increases as pH increases. A structural index of '1.0' would represent a perfect sphere (mean \pm SEM, $n=13$ experiments). (C) At pH 6.8 cells show a spindle-like morphology. They become spherical as the extracellular pH increases to pH 7.5 (scale bar, 50 μm). (D and E) Both migratory speed (D) and the translocation over a period of 5 hours (E) reach their maxima at pH 7.0. Inhibition of NHE1 with cariporide reduces the migratory speed and the displacement at pH_e 7.0 and 7.5 while at pH_e 6.8 it has no statistically significant effect (mean \pm SEM; n per value = at least 30 cells from 8 experiments). (F) Invasion through a coated filter membrane depends on extracellular pH with a maximum invasion at pH_e 7.0. It is completely blocked when NHE1 is inhibited (mean \pm SEM; $n=8$ independent experiments).

present study, laminin and fibronectin were key constituents of the basement membrane-like matrix. Both laminin and fibronectin can be bound by heparin or heparan sulfate present at the cell surface as a component of the glycocalyx (42-44).

Heparan sulfate proteoglycans also represent specific components of native basement membranes and the degradation of heparan sulfate chains is required for B16 cell invasion (40). Our reconstituted basement membrane-like matrix used here

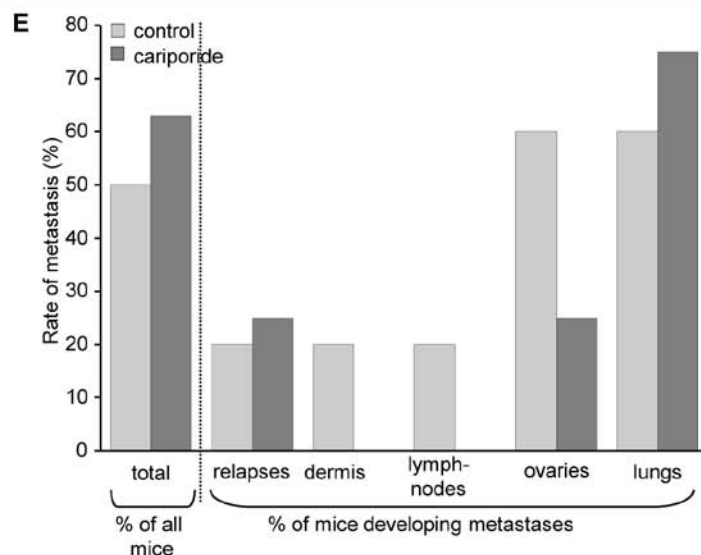
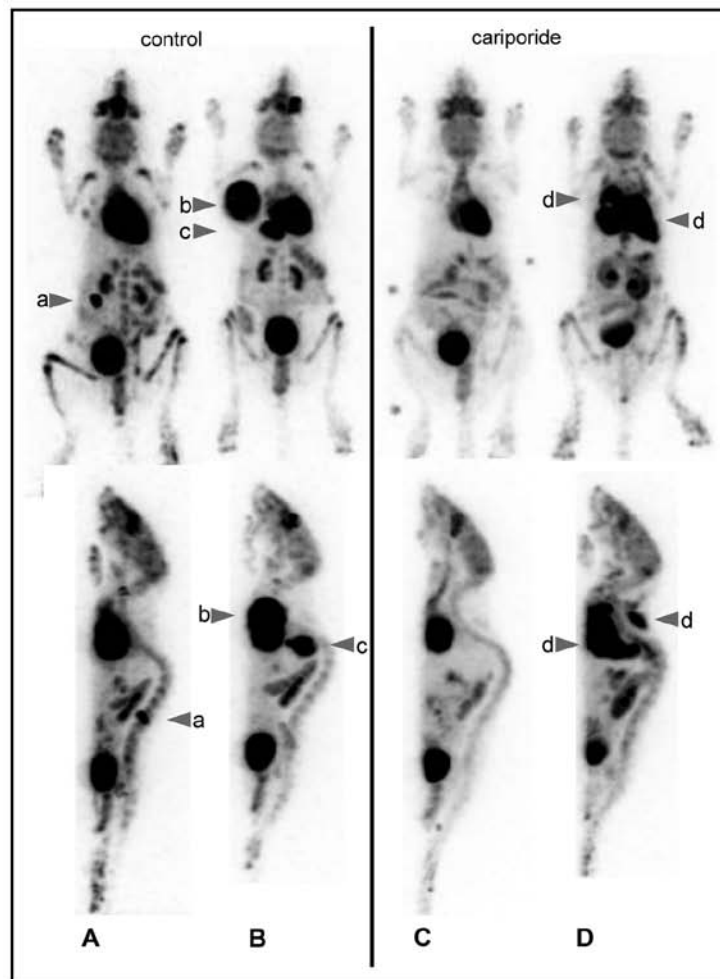


Figure 7. B16V metastasis in female C57BL/6 mice fed on a standard (A, B and E; n=8) or a cariporide (C, D and E; n=8) containing diet. Three weeks after intradermal injection of a B16V cell suspension into the right flank, the primary tumor was removed and metastasis was monitored over a period of 7 weeks employing a small-animal PET. Fluorodeoxy-glucose indicates metastases by accumulating in metabolically active organs and tissues. The PET monitoring (shown as maximum intensity projections) was followed by autopsies of the sacrificed animals. (A) Ovarian metastasis (a). (B) Axillary lymph node (b) and pulmonary metastasis (c). (C) Animal without metastases. (D) Pulmonary metastases (d). (E) The percentage of animals developing metastases or recrudescence hardly differs between the two groups. However, in cariporide treated animals metastases appear to get directed to the lungs while animals feeding on the standard diet show metastases spread all over the body.

did not contain any heparan sulfate proteoglycans which could account for the lack of invasion (Fig. 4F).

B16V cell adhesion was twice as strong on the basement membrane- as on the dermis-like matrix (Fig. 4B). This strong

adhesion to the basement membrane can be correlated with a rather low translocation (Fig. 4D) as the cells keep moving vividly, although on the spot (Fig. 4C). $\alpha_4\beta_1$, $\alpha_6\beta_1$ and $\alpha_v\beta_3$ integrins preferentially bind to collagen IV, laminin and fibronectin, respectively (45,46), and in murine melanoma cells, $\alpha_v\beta_3$ integrin-binding to fibronectin mediates adhesion and motility (47,48). Thus, the components of the reconstituted basement membrane force the cells to use the appropriate integrin dimers in order to interact specifically with the respective constituent. The present reconstituted basement membrane induced adhesion and spreading but did not facilitate translocation and invasion (Fig. 4) suggesting that either the $\alpha_v\beta_3$ integrin-binding to fibronectin was too strong or that in addition other cell-matrix interactions are required for directional migration or invasion.

The ECM composition determines the efficiency of NHE1 inhibition. Both migration and invasion of human melanoma (MV3) cells require well-balanced adhesion strength and depend on NHE1 activity and pH_e (31,49). B16V cell adhesion and migration on the dermis-like matrix also depend on pH_e and NHE1 activity (Fig. 6A-E). The higher the extracellular proton concentration is the stronger is the adhesion strength, and adhesion is clearly reduced when NHE1 is inhibited by cariporide. The cariporide-induced decrease in motility can be compensated for by an increase in the extracellular H^+ concentration, i.e. a decrease in pH_e , especially visible at pH_e 6.8 (Fig. 6D and E).

In MV3 cells NHE1 modulates the cell surface pH (8,15), even locally right next to integrins at focal adhesions (24). These pH-environments are stabilized by the glycocalyx (23). Particularly at focal adhesions at the cell front, the pericellular H^+ concentration is high. An acidic extracellular pH activates $\alpha_v\beta_3$ integrins by opening the head pieces of the dimers (50). Thus, the protons extruded by NHE1, predominantly at focal adhesions, could stabilize the $\alpha_v\beta_3$ integrin-mediated B16V cell adhesion on the basement membrane-like matrix. Indeed, NHE1 inhibition by cariporide reduces adhesion by more than 50% (Fig. 4B).

The high levels of basal NHE1 activity in tumor cells (10,51) and the resulting acidification of both the cell surface and the extracellular space also elevate the proteolytic potential leading to an increase of tumor cell invasiveness (22). A low pH_e of the tumor microenvironment optimizes the activity of matrix metalloproteinases (MMPs) (52) and cathepsins D (53,54), B and L (55) as well as the urokinase-type plasminogen activator (56). In this context, even $\alpha_v\beta_3$ integrin expression might facilitate B16 cell invasion of collagen type I-containing matrices. Collagen type I, denatured by heat or after proteolysis at physiological temperatures can be ligated by $\alpha_v\beta_3$ integrins (57). Thus, initial, unspecific digestion of dermal collagen type I during the course of tissue remodeling or infiltration makes cryptic RGD sites accessible (58) for $\alpha_v\beta_3$ integrins. The stimulated $\alpha_v\beta_3$ integrins activate MMP2 present on the cell surface which in turn furthers collagen type I digestion (59). The proteolytic activity of MMPs was indeed significantly higher in cells seeded on a dermis-like matrix (Fig. 5) strongly suggesting that the molecular composition and/or the structure of the ECM trigger its own digestion. A considerable role of NHE1 activity in this setting is supported by the present findings that on the

dermis-like matrix the proteolytic activity is significantly reduced and the invasion nearly completely blocked upon NHE1 inhibition. However, during invasion as opposed to migration, a missing NHE1 activity cannot be compensated for by a decrease in pH_e (Fig. 6F) confirming that the protons locally extruded by NHE1 dominate those present in the bulk solution (15).

NHE1 inhibition is ineffective in the lungs. In mice, NHE1 inhibition does not inhibit the overall metastasis rate but seems to direct metastasis preferentially to the lungs (Fig. 7B), or put differently, cariporide does not inhibit metastasis to the lungs. Two factors could contribute to this phenomenon: i) the composition of the lung ECM may support homing; and ii) the local, alveolar pCO_2 and hence the local pH_e might circumvent the blockade of NHE1.

The ECM of the lung is a network of non-uniformly distributed elastic fibers that loop around alveolar ducts and form rings at the mouths of alveoli (60). It consists of elastin, a highly proteinase-resistant protein, interstitial collagen types I and III that provide tensile strength, and collagen type IV as part of the basement membrane separating the alveolar endothelium and epithelium. Also in the lungs proteoglycans, in particular the heparan-sulfate proteoglycan whose degradation is required for B16 cell invasion (40), are highly expressed in both the basement membrane and the interstitium (60,61). Furthermore, numerous studies indicate that fibronectin, the preferential ligand of $\alpha_v\beta_3$ integrins, is present in the basement membrane of alveolar epithelia (reviewed in ref. 62). Spontaneous metastasis of breast cancer to lung and bone is enhanced by $\alpha_v\beta_3$ integrins, partially due to their strong binding to fibronectin and vitronectin (63-65). In addition, binding of $\alpha_v\beta_3$ integrins to ECM proteins prevents apoptosis in a foreign environment (66).

In a healthy human being pH_e values come to about pH 7.1 in liver, less than pH 6.9 in active muscle, and only pH 6.7 in the pulmonary extracellular space (67). The *in vitro* experiments of the present study show that regarding cell motility (Fig. 6D and E) the proton concentration at a pH_e of 6.8 appears to compensate for NHE1 inhibition. Consequently, the rather acidic pH in the extravascular space of the lung could neutralize the effects of NHE1 inhibition by cariporide which then would lead to the observed formation of lung metastases in the cariporide treated mice.

Although NHE1 inhibition leads to a decrease in adhesion, invasion and metastasis, its function as a sole potential target in cancer therapy remains still questionable. The present results show that the effectiveness of NHE1 inhibition in reducing melanoma metastasis depends on both the composition of the ECM, which varies tremendously between different organs and tissues, and the local pH_e , which is modulated by NHE1 activity, vascularization, pCO_2 and other acid/base regulators. The locally very different interstitial pH_e values depend not only on the local metabolism and vascularization/perfusion but also on the buffer capacity determined by the local, tissue-specific glycosaminoglycan composition. Due to the interweaving of these numerous parameters it will be very difficult to analyze and predict the efficacy of NHE1 inhibition locally and individually. Nevertheless, the use of NHE1 inhibitors as an adjuvant therapy strategy or as one constituent of a broader drug cocktail appears to be a promising approach to further advance anticancer therapies.

Acknowledgements

The authors thank Dr Steve J. Reshkin (University of Bari) and Dr Uta Schnöckel (UKM) for providing their expertise on *in situ* zymography and the PET technique, respectively. Christine Bätza and Anne Kanzog performed the PET procedure. Sincere thanks also to Dr Jürgen Pünter at Sanofi-Aventis for kindly providing cariporide. This study was supported by the Interdisciplinary Center of Clinical Research (IZKF core unit PIX), University of Münster, Germany.

References

- Lock JG, Wehrle-Haller B and Stromblad S: Cell-matrix adhesion complexes: master control machinery of cell migration. *Semin Cancer Biol* 18: 65-76, 2008.
- Broussard JA, Webb DJ and Kaverina I: Asymmetric focal adhesion disassembly in motile cells. *Curr Opin Cell Biol* 20: 85-90, 2008.
- Arnaout MA, Goodman SL and Xiong JP: Structure and mechanics of integrin-based cell adhesion. *Curr Opin Cell Biol* 19: 495-507, 2007.
- Niggli V and Rossy J: Ezrin/radixin/moesin: versatile controllers of signaling molecules and of the cortical cytoskeleton. *Int J Biochem Cell Biol* 40: 344-349, 2008.
- Grinstein S, Woodside M, Waddell TK, *et al.*: Focal localization of the NHE-1 isoform of the Na⁺/H⁺ antiporter: assessment of effects on intracellular pH. *EMBO J* 12: 5209-5218, 1993.
- Plopper GE, McNamee HP, Dike LE, Bojanowski K and Ingber DE: Convergence of integrin and growth factor receptor signaling pathways within the focal adhesion complex. *Mol Biol Cell* 6: 1349-1365, 1995.
- Stock C and Schwab A: Role of the Na/H exchanger NHE1 in cell migration. *Acta Physiol (Oxf)* 187: 149-157, 2006.
- Stock C, Mueller M, Kraehling H, *et al.*: pH nanoenvironment at the surface of single melanoma cells. *Cell Physiol Biochem* 20: 679-686, 2007.
- Harguindey S, Orive G, Luis Pedraz J, Paradiso A and Reshkin SJ: The role of pH dynamics and the Na⁺/H⁺ antiporter in the etiopathogenesis and treatment of cancer. Two faces of the same coin - one single nature. *Biochim Biophys Acta* 1756: 1-24, 2005.
- Stock C, Ludwig FT and Schwab A: Is the multifunctional Na⁺/H⁺ exchanger isoform 1 a potential therapeutic target in cancer? *Curr Med Chem* 19: 647-660, 2012.
- Warburg O: On the origin of cancer cells. *Science* 123: 309-314, 1956.
- Helmlinger G, Sckell A, Dellian M, Forbes NS and Jain RK: Acid production in glycolysis-impaired tumors provides new insights into tumor metabolism. *Clin Cancer Res* 8: 1284-1291, 2002.
- Meima ME, Mackley JR and Barber DL: Beyond ion translocation: structural functions of the sodium-hydrogen exchanger isoform-1. *Curr Opin Nephrol Hypertens* 16: 365-372, 2007.
- Klein M, Seeger P, Schuricht B, Alper SL and Schwab A: Polarization of Na⁺/H⁺ and Cl⁻/HCO₃⁻ exchangers in migrating renal epithelial cells. *J Gen Physiol* 115: 599-608, 2000.
- Stuwe L, Muller M, Fabian A, *et al.*: pH dependence of melanoma cell migration: protons extruded by NHE1 dominate protons of the bulk solution. *J Physiol* 585: 351-360, 2007.
- Cardone RA, Bellizzi A, Busco G, *et al.*: The NHERF1 PDZ2 domain regulates PKA-RhoA-p38-mediated NHE1 activation and invasion in breast tumor cells. *Mol Biol Cell* 18: 1768-1780, 2007.
- Bourguignon LY, Singleton PA, Diedrich F, Stern R and Gilad E: CD44 interaction with Na⁺-H⁺ exchanger (NHE1) creates acidic microenvironments leading to hyaluronidase-2 and cathepsin B activation and breast tumor cell invasion. *J Biol Chem* 279: 26991-27007, 2004.
- Hu G, Kang Y and Wang XF: From breast to the brain: unraveling the puzzle of metastasis organotropism. *J Mol Cell Biol* 1: 3-5, 2009.
- Meyers ML and Balch CM: Diagnosis and treatment of metastatic melanoma. In: *Cutaneous Melanoma*. Balch CM, Houghton AN, Sober AJ and Soong S-J (eds.) Quality Medical Publishing, Inc., St. Louis, MO, 1998.
- Paget S: The distribution of secondary growths in cancer of the breast. 1889. *Cancer Metastasis Rev* 8: 98-101, 1989.
- Peyton SR and Putnam AJ: Extracellular matrix rigidity governs smooth muscle cell motility in a biphasic fashion. *J Cell Physiol* 204: 198-209, 2005.
- Stock C, Cardone RA, Busco G, Kraehling H, Schwab A and Reshkin SJ: Protons extruded by NHE1: digestive or glue? *Eur J Cell Biol* 87: 591-599, 2008.
- Kraehling H, Mally S, Eble JA, Noel J, Schwab A and Stock C: The glycocalyx maintains a cell surface pH nanoenvironment crucial for integrin-mediated migration of human melanoma cells. *Pflügers Arch* 458: 1069-1083, 2009.
- Ludwig FT, Schwab A and Stock C: The Na⁺/H⁺ - exchanger (NHE1) generates pH nanodomains at focal adhesions. *J Cell Physiol* 228: 1351-1358, 2013.
- Supino R, Prosperi E, Formelli F, Mariani M and Parmiani G: Characterization of a doxorubicin-resistant murine melanoma line: studies on cross-resistance and its circumvention. *Br J Cancer* 54: 33-42, 1986.
- Fafournoux P, Noel J and Pouyssegur J: Evidence that Na⁺/H⁺ exchanger isoforms NHE1 and NHE3 exist as stable dimers in membranes with a high degree of specificity for homodimers. *J Biol Chem* 269: 2589-2596, 1994.
- Haier J, Korb T, Hotz B, Spiegel HU and Senninger N: An intravital model to monitor steps of metastatic tumor cell adhesion within the hepatic microcirculation. *J Gastrointest Surg* 7: 507-515, 2003.
- Korb T, Schluter K, Enns A, *et al.*: Integrity of actin fibers and microtubules influences metastatic tumor cell adhesion. *Exp Cell Res* 299: 236-247, 2004.
- Busco G, Cardone RA, Greco MR, *et al.*: NHE1 promotes invadopodial ECM proteolysis through acidification of the peri-invadopodial space. *FASEB J* 24: 3903-3915.
- Schafers KP, Reader AJ, Kriens M, Knoess C, Schober O and Schafers M: Performance evaluation of the 32-module quadHIDAC small-animal PET scanner. *J Nucl Med* 46: 996-1004, 2005.
- Stock C, Gassner B, Hauck CR, *et al.*: Migration of human melanoma cells depends on extracellular pH and Na⁺/H⁺ exchange. *J Physiol* 567: 225-238, 2005.
- Couvelard A, Scoazec JY, Dauge MC, Bringuier AF, Potet F and Feldmann G: Structural and functional differentiation of sinusoidal endothelial cells during liver organogenesis in humans. *Blood* 87: 4568-4580, 1996.
- Poincloux R, Lizarraga F and Chavrier P: Matrix invasion by tumour cells: a focus on MT1-MMP trafficking to invadopodia. *J Cell Sci* 122: 3015-3024, 2009.
- Roy R, Yang J and Moses MA: Matrix metalloproteinases as novel biomarkers and potential therapeutic targets in human cancer. *J Clin Oncol* 27: 5287-5297, 2009.
- Bedossa P and Paradis V: Liver extracellular matrix in health and disease. *J Pathol* 200: 504-515, 2003.
- Martinez-Hernandez A: The hepatic extracellular matrix. I. Electron immunohistochemical studies in normal rat liver. *Lab Invest* 51: 57-74, 1984.
- Rosenow F, Ossig R, Thormeyer D, *et al.*: Integrins as antimetastatic targets of RGD-independent snake venom components in liver metastasis [corrected]. *Neoplasia* 10: 168-176, 2008.
- Schuppan D: Structure of the extracellular matrix in normal and fibrotic liver: collagens and glycoproteins. *Semin Liver Dis* 10: 1-10, 1990.
- Gressner AM: Hepatic proteoglycans - a brief survey of their pathobiochemical implications. *Hepatogastroenterology* 30: 225-229, 1983.
- Kramer RH and Vogel KG: Selective degradation of basement membrane macromolecules by metastatic melanoma cells. *J Natl Cancer Inst* 72: 889-899, 1984.
- Luikart SD, Maniglia CA and Sartorelli AC: Influence of collagen substrata on glycosaminoglycan production by B16 melanoma cells. *Proc Natl Acad Sci USA* 80: 3738-3742, 1983.
- Culp LA, Rollins BJ, Buniel J and Hitri S: Two functionally distinct pools of glycosaminoglycan in the substrate adhesion site of murine cells. *J Cell Biol* 79: 788-801, 1978.
- Yamada KM, Kennedy DW, Kimata K and Pratt RM: Characterization of fibronectin interactions with glycosaminoglycans and identification of active proteolytic fragments. *J Biol Chem* 255: 6055-6063, 1980.
- Sakashita S, Engvall E and Ruoslahti E: Basement membrane glycoprotein laminin binds to heparin. *FEBS Lett* 116: 243-246, 1980.

45. Ramos DM, Berston ED and Kramer RH: Analysis of integrin receptors for laminin and type IV collagen on metastatic B16 melanoma cells. *Cancer Res* 50: 728-734, 1990.
46. Tietze L, Borntraeger J, Klosterhalfen B, *et al*: Expression and function of beta(1) and beta(3) integrins of human mesothelial cells in vitro. *Exp Mol Pathol* 66: 131-139, 1999.
47. Lonsdorf AS, Kramer BF, Fahrleitner M, *et al*: Engagement of α IIb β 3 (GPIIb/IIIa) with α v β 3 integrin mediates interaction of melanoma cells with platelets: a connection to hematogenous metastasis. *J Biol Chem* 287: 2168-2178, 2012.
48. Li X, Regezi J, Ross FP, *et al*: Integrin alphavbeta3 mediates K1735 murine melanoma cell motility in vivo and in vitro. *J Cell Sci* 114: 2665-2672, 2001.
49. Friedl P, Maaser K, Klein CE, Niggemann B, Krohne G and Zanker KS: Migration of highly aggressive MV3 melanoma cells in 3-dimensional collagen lattices results in local matrix reorganization and shedding of alpha2 and beta1 integrins and CD44. *Cancer Res* 57: 2061-2070, 1997.
50. Paradise RK, Lauffenburger DA and Van Vliet KJ: Acidic extracellular pH promotes activation of integrin alpha(v) beta(3). *PLoS One* 6: e15746, 2011.
51. Cardone RA, Casavola V and Reshkin SJ: The role of disturbed pH dynamics and the Na⁺/H⁺ exchanger in metastasis. *Nat Rev Cancer* 5: 786-795, 2005.
52. Koblinski JE, Ahram M and Sloane BF: Unraveling the role of proteases in cancer. *Clin Chim Acta* 291: 113-135, 2000.
53. Tedone T, Correale M, Barbarossa G, Casavola V, Paradiso A and Reshkin SJ: Release of the aspartyl protease cathepsin D is associated with and facilitates human breast cancer cell invasion. *FASEB J* 11: 785-792, 1997.
54. Szpaderska AM and Frankfater A: An intracellular form of cathepsin B contributes to invasiveness in cancer. *Cancer Res* 61: 3493-3500, 2001.
55. Mohamed MM and Sloane BF: Cysteine cathepsins: multifunctional enzymes in cancer. *Nat Rev Cancer* 6: 764-775, 2006.
56. Kindzelskii AL, Amhad I, Keller D, *et al*: Pericellular proteolysis by leukocytes and tumor cells on substrates: focal activation and the role of urokinase-type plasminogen activator. *Histochem Cell Biol* 121: 299-310, 2004.
57. Pauli BU and Knudson W: Tumor invasion: a consequence of destructive and compositional matrix alterations. *Hum Pathol* 19: 628-639, 1988.
58. Taubenberger AV, Woodruff MA, Bai H, Muller DJ and Hutmacher DW: The effect of unlocking RGD-motifs in collagen I on pre-osteoblast adhesion and differentiation. *Biomaterials* 31: 2827-2835, 2010.
59. Brooks PC, Stromblad S, Sanders LC, *et al*: Localization of matrix metalloproteinase MMP-2 to the surface of invasive cells by interaction with integrin alpha v beta 3. *Cell* 85: 683-693, 1996.
60. Shapiro SD: Chairman's summary. In: *Proceedings of the American Thoracic Society*, p4, 2006.
61. Thompson SM, Jesudason EC, Turnbull JE and Fernig DG: Heparan sulfate in lung morphogenesis: The elephant in the room. *Birth Defects Res C Embryo Today* 90: 32-44, 2010.
62. Dunsmore SE and Rannels DE: Extracellular matrix biology in the lung. *Am J Physiol* 270: L3-L27, 1996.
63. Harms JF, Welch DR, Samant RS, *et al*: A small molecule antagonist of the alpha(v)beta3 integrin suppresses MDA-MB-435 skeletal metastasis. *Clin Exp Metastasis* 21: 119-128, 2004.
64. Sloan EK, Pouliot N, Stanley KL, *et al*: Tumor-specific expression of alphavbeta3 integrin promotes spontaneous metastasis of breast cancer to bone. *Breast Cancer Res* 8: R20, 2006.
65. Bentmann A, Kawelke N, Moss D, *et al*: Circulating fibronectin affects bone matrix, whereas osteoblast fibronectin modulates osteoblast function. *J Bone Miner Res* 25: 706-715, 2010.
66. Montgomery AM, Reisfeld RA and Cheresch DA: Integrin alpha v beta 3 rescues melanoma cells from apoptosis in three-dimensional dermal collagen. *Proc Natl Acad Sci USA* 91: 8856-8860, 1994.
67. Effros RM and Chinard FP: The in vivo pH of the extravascular space of the lung. *J Clin Invest* 48: 1983-1996, 1969.